

Type of Hip Fracture Determines Load Share in Intramedullary Osteosynthesis

Sebastian Eberle MS, Claus Gerber MS,
Geert von Oldenburg MS, Sven Hungerer MD,
Peter Augat PhD

Published online: 31 March 2009
© The Association of Bone and Joint Surgeons 2009

Abstract The choice of the appropriate implant continues to be critical for fixation of unstable hip fractures. Therefore, the goal of this study was to develop a numerical model to investigate the mechanical performance of hip fracture osteosynthesis. We hypothesized that decreasing fracture stability results in increasing load share of the implant and therefore higher stress within the implant. We also investigated the relationship of interfragmentary movement to the fracture stability. A finite element model was developed for a cephalomedullary nail within a synthetic femur and simulated a pertrochanteric fracture, a lateral neck fracture, and a subtrochanteric fracture. The femur was loaded with a hip force and was constrained physiologically. The FE model was validated by mechanical experiments. All three fractures resulted in similar values for stiffness (462–528 N/mm). The subtrochanteric fracture resulted in the highest local stress (665 MPa), and the pertrochanteric fracture resulted in a lower stress (621 MPa) with even lower values for the lateral neck fracture (480 MPa). Thus, intramedullary implants can stabilize unstable hip fractures with almost the same amount of stiffness as seen in stable fractures, but they have to bear a higher load share, resulting in higher stresses in the implant.

Introduction

Due to an ever-aging population and an increasing prevalence of osteoporosis, the number of hip fractures is increasing [10]. With about 1.7 million hip fractures worldwide in 1990, the projected estimate for the number of hip fractures in 2050 ranges from 4.5 to 6.3 million with pessimistic calculations amounting to 21.3 million [9, 14]. These fractures are associated with a mortality between 10% and 20%, functional disability, and a loss of mobility and independence [4, 13]. Thus hip fractures have a negative impact on the patient's life and on healthcare costs. Methods to improve the medical care for these patients that allow early mobilization and a fast return to prefracture levels of independence are required.

Although method-specific complications (eg, failure of the implant) and delayed fracture healing are rare, they occur in up to 12.6% of hip fracture patients and usually require surgical revision [24]. A large variety of implants for the treatment of hip fractures is available to address these types of complications. Implants are typically employed to fix a certain range of different fracture types (eg, cephalomedullary nails for intertrochanteric and subtrochanteric fractures). However, different fracture types have shown to result in different stabilities of the osteosynthesis. Yet the stability of the osteosynthesis is not necessarily related to the stability of the initial fracture situation [3, 15, 23]. With decreasing fracture stability, the load on the bone decreases and the load on the implant increases [3, 5, 16, 17, 26].

If stable fractures are fixed with various implants, there are only minor differences in the rigidities of the osteosynthesis [25]. However, if different implants are used for unstable fractures (eg, comminution, segmental bone loss) there might be considerable differences in the rigidity of

Claus Gerber and Geert von Oldenburg are employees of Stryker Osteosynthesis. Peter Augat receives research funding from Stryker Osteosynthesis and B.Braun Melsungen AG.

S. Eberle (✉), S. Hungerer, P. Augat
Institute of Biomechanics, Trauma Center Murnau,
Prof. Küntscher Str. 8, 82418 Murnau, Germany
e-mail: sebastian.eberle@bgu-murnau.de

C. Gerber, G. von Oldenburg
Stryker Osteosynthesis, Schoenkirchen/Kiel, Germany

the osteosynthesis [16, 25]. So the choice of the implant is particularly critical in unstable fractures. This is reflected in the clinical situation where the failure rate in unstable fractures is significantly increased compared to stable fractures [1, 21, 29]. Although these complications in unstable fractures are largely related to the local mechanical situation at the fracture site, no standardized biomechanical model exists to study the mechanical characteristics of hip fracture osteosynthesis [12].

The goal of this study was to develop a numerical model of a standardized synthetic human femur with an implanted intramedullary nail and validate it by strain measurements on the nail to study the mechanical characteristics of hip fracture osteosynthesis. We hypothesized that decreasing fracture stability results in increasing load share of the implant and therefore higher stress within the implant. We further wanted to investigate how the amount of movement between the fracture fragments is related to the fracture stability.

Materials and Methods

To examine the load share in intramedullary osteosynthesis of hip fractures, a finite element (FE) model was developed for a cephalomedullary nail within a synthetic femur. The FE model consisted of the digital model of a Gamma3 Trochanteric Nail 180 (Stryker Osteosynthesis, Schoenkirchen/Kiel, Germany) and the so-called standardized femur [11]. The standardized femur is a 3-D solid model derived from a CT-scan dataset of a large left third-generation synthetic femur (model 3306, Sawbones AB, Malmo, Sweden) made available in the public domain [6]. This model differentiates between cortical and cancellous bone and includes an intramedullary canal.

The material properties for the synthetic femur were assigned according to the manufacturer's specifications for a fourth-generation Sawbone (model 3406), which has exactly the same geometry as the third-generation femur but improved material properties. The Young's modulus was set to 16 GPa for cortical bone and to 104 MPa for cancellous bone, respectively. A Poisson's ratio of 0.3 was assigned for both bone materials. For the cephalomedullary implant, consisting of a nail, lag screw, and distal locking screw, the material properties of TiAl6V4 were employed. The Young's modulus was set to 113.8 GPa and the Poisson's ratio to 0.34. All materials were assumed to be homogeneous, isotropic, and linear elastic.

Boolean operations were used to mimic the drilling and reaming process required for the insertion of the implant. Boolean operations are logical operations like add, subtract or intersect on combinations of geometric entities. In this case the volumes defined by the outer shape of the rotating

drills used in the operative procedure were subtracted from the bone. The cavities that were created in the bone by the Boolean operations corresponded exactly to the cavities occurring in a real surgery according to the operative technique provided by the manufacturer. The exact position of the implant within the synthetic femur was verified using exemplary radiographs from the later mechanical experiments. The hip fractures to be studied were inserted by means of virtual osteotomies without leaving a residual gap between the fracture fragments. Three different fractures were investigated (Fig. 1A–C): a pertrochanteric fracture (AO 31A1.1), a lateral neck fracture (AO 31B2.1), and a subtrochanteric fracture (AO 31A3.2).

Loading of the femur was performed with a single hip force with physiological constraints at the femoral head and at the distal end. The hip force was calculated according to Bergmann et al. for an 80 kg person and amounted to 1866 N [2]. This force displayed the maximum load during the human walking cycle acting on the femoral head. This scenario was chosen because walking is the most common loading case during the recovery of patients with an occurrence of 10.2% in contrast to climbing or descending stairs with 0.4% [18]. The force was introduced to the center of the femoral head that was constrained in the plane orthogonal to the force vector (Fig. 2A–B). The distal end of the bone was constrained in all translational degrees of freedom (DOF) at a point in the frontal plane. This pivotal point was located at the medial condyle 23 mm from the shaft axis [19]. The bone was able to rotate about this pivotal point about the frontal and the sagittal axis.

The FE models had about 30,000 elements and 60,000 nodes and were created using ANSYS® Academic Research, v.11.0 Workbench™ (ANSYS Inc., Canonsburg, PA). Higher-order (quadratic ansatz) structural solids with hexahedral or tetrahedral shapes were used, depending on the geometry to be meshed. Convergence tests were performed on all models to assure that a fine enough element discretization has been used for stress analysis.

All contacts between the two fracture fragments and the implant were considered. All contacts were modeled as frictional contacts except the interfaces between the threaded parts of implant and bone. These interfaces were modeled as bonded contacts as the screw connections did not allow axial or shear movement and the screws were not of any special interest (eg, stress in the thread). The coefficients of friction for the frictional contacts were 0.46 for the pairing of bone-bone (determined in own experiments, unpublished), 0.23 for implant-implant (determined in own experiments, unpublished), and 0.3 for implant-bone [20]. The contacts were calculated with an Augmented Lagrange algorithm and a factor-based contact stiffness. The Augmented Lagrange method modeled Coulomb friction

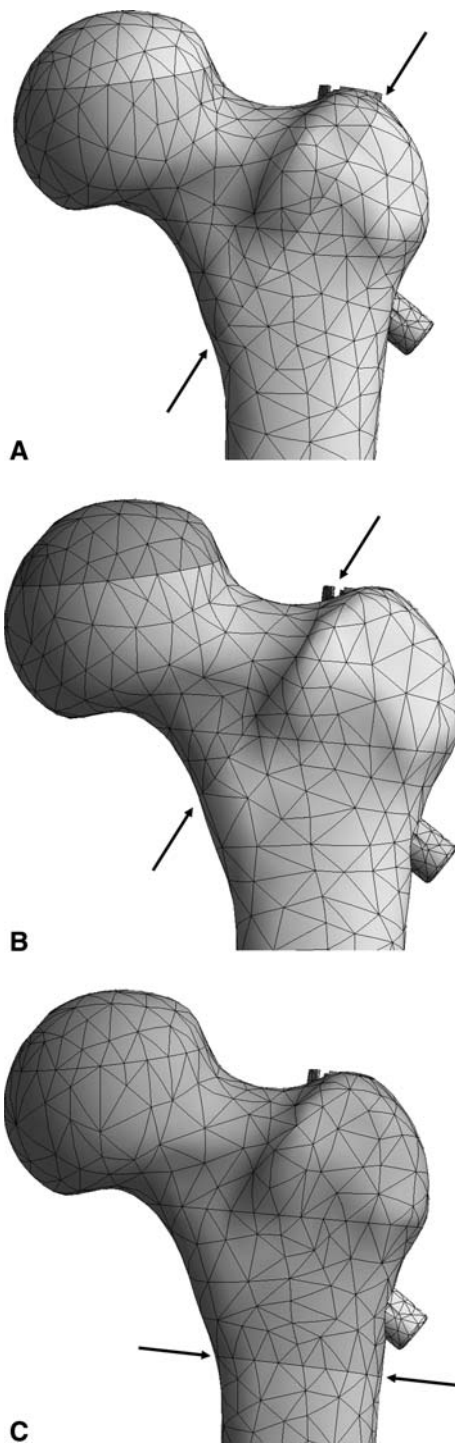


Fig. 1A–C The three fractures used for the FE simulations are shown. The arrows mark the line of fracture for the pertrochanteric fracture (A), the lateral neck fracture (B) and the subtrochanteric fracture (C).

behavior. The algorithm transmitted pressure in normal direction and frictional stresses in tangential direction and therefore allowed sticking and slipping depending on the static friction coefficient and the normal force between the

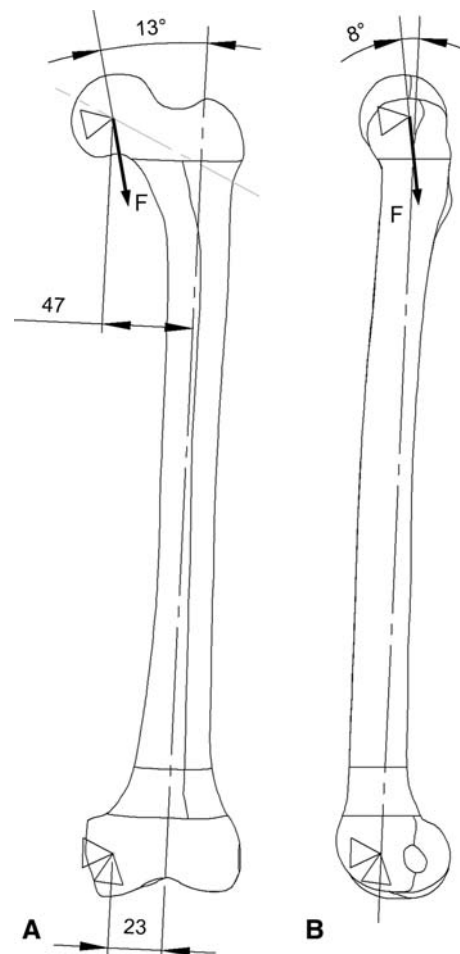


Fig. 2A–B The boundary conditions for the FE model are shown. The vector of the single hip force (F) with its angles in the frontal (A) and in the sagittal (B) plane are illustrated.

two contacting bodies. The contact stiffness was updated in every iteration to improve convergence behavior.

To determine the stiffness of the whole osteosynthesis, the maximum load was divided by the maximum displacement of the center of the femoral head in the load direction. The Von Mises stress distribution within the nail and the lag screw was examined to identify the location and the magnitude of the maximum Von Mises stress in regions of high tensile strain in axial direction of the nail. By doing so, stress points could be identified, which were susceptible to failure. The interfracture movement (IFM) was evaluated by calculating the maximum axial and transverse displacement between the two fracture fragments. The IFM was defined as the relative motion of the centers of area of the two fracture fragments' areas that were in apposition. For the later validation the maximum normal strain on the nail in the direction of the longitudinal axis of the nail was calculated.

In order to test the sensitivity of the FE model on the effects of implant position and the coefficients of friction, a

parameter study was conducted. The implant position was varied by altering the frontal angle ($+0.5^\circ$ or -1.0°) of the nail in the bone and the coefficient of friction in the fracture gap ($\mu = 0.1-0.8$). Because the coefficient of friction for the pairing of implant and bone was derived from the literature for a different synthetic material than the cancellous bone that was used, this parameter was changed as well ($\mu = 0.1-0.8$).

To validate the FE model, experiments were conducted according to the assembly and the load scenario of the FE simulations. Eighteen large left fourth-generation Sawbones were tested (model 3406, Sawbones AB, Malmo, Sweden) that were osteomized and fixed with Gamma3 trochanteric nails 180. For the purpose of validation, strains were recorded on the nail with strain gauges during loading. The specimens were divided into three groups before testing. Each group ($n = 6$) was assigned to one of the previous simulated hip fractures. The fractures were realized by means of osteotomies with a guided handsaw and a cutting template. The cutting template assured the reproducibility of the fractures.

The surgery followed the usual operative technique for the Gamma3 trochanteric nail without intramedullary reaming and was conducted by an experienced surgeon. The surgery started with the proximal opening of the femur by a one-step conical reamer. For the drilling of the hole for the lag screw, a dummy nail of equal dimensions to the implanted nail was inserted. The nail was inserted first, followed by the lag screw positioned central with its tip in the femoral head, and the distal locking screw. The lateral neck fracture was locked statically and the other two fractures were locked dynamically, following clinical practice. No gap size was left between the fracture fragments.

Before implantation, the nails were supplied with three uniaxial strain gauges. The strain gauges (KFG-1-120-C1-11L3M3R, Kyowa Electronic Instruments Co., Ltd., Tokyo, Japan) were glued to the proximal lateral part of the nail anterior and posterior to the aperture for the lag screw and to the lateral side of the nail shaft (Fig. 3A–B).

These positions were determined in the previous numerical simulations as areas of high equivalent stress. The axes of all strain gauges were aligned with the longitudinal axis of the nail particularly to measure strains deriving from bending of the nail. The three strain gauges were connected to the data acquisition system Spider 8 (Hottinger Baldwin Messtechnik GmbH, Germany) that was linked to a personal computer to record the data with the software Catman easy (Hottinger Baldwin Messtechnik GmbH, Germany).

Subsequent to the surgery, the specimens were embedded in PMMA at the distal end and at the head. The femoral head was embedded in a hemisphere of PMMA,

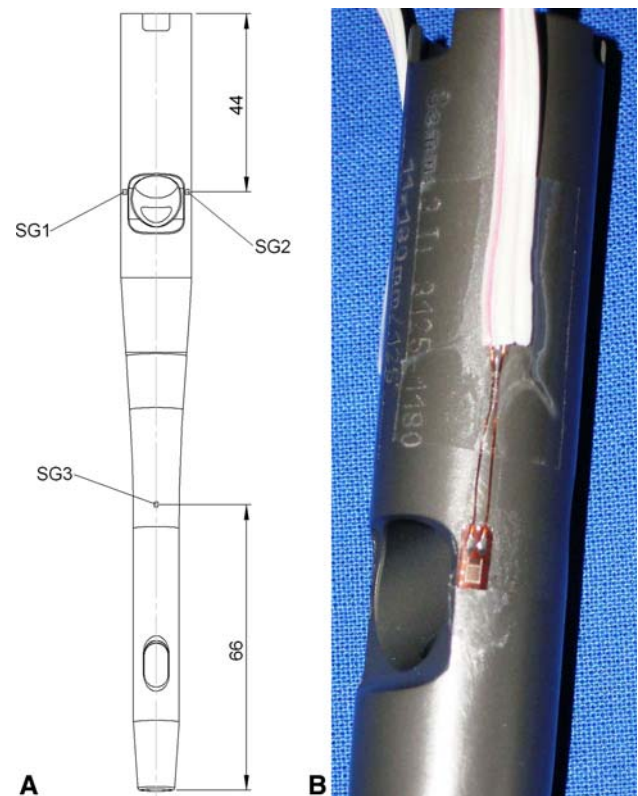


Fig. 3A–B (A) The positions of the strain gauges SG1 to SG3 on the nail are shown. (B) A strain gauge with its cable applied next to the lag screw hole is shown.

which fit into the hemispherical adapter of the test jig. Due to the concentricity of the head, PMMA, and adapter, the force of the testing machine was aligned through the center of the femoral head. The distal end of the bone was embedded in a two-part cast made of PMMA.

The embedded sawbones were mounted into an axial load test jig of a servo-electric testing machine (Zwick 010, Zwick GmbH & Co. KG, Germany). The testing machine introduced the machine force by a ball-joint-like support to the femoral head (Fig. 4). The distal end was supported by a universal joint with two axes. The angles between the machine force and the bone shaft axis were 13° in the frontal and 8° in the sagittal plane according to Bergmann et al. [2]. The load offsets to the diaphyseal axis were 47 mm proximally and 23 mm distally, respectively. Thus, the test setup matched exactly the boundary and loading conditions of the FE simulations.

Static tests were performed with elastic deformation of the specimens. No plastic deformation or fracture of the specimens occurred. The tests were displacement controlled and conducted with a velocity of 10 mm/min. The testing procedure included several load cycles (Table 1) up to a maximum force of 1866 N. The load levels were controlled via a 10 kN load cell (Serie K, GTM Gassmann

Testing and Metrology GmbH, Germany) fixed to the load piston of the testing machine. The cyclic loading had the purpose to precondition the osteosynthesis. The holding time assured to measure strains and displacement without any delayed effects. As reported by Cristofolini et al. whole bone composite femur models should be held for 4 min at the maximum load to exclude any effects of creepage [11].

The load versus deformation curve was recorded for the full load range and for all test cycles to determine the axial stiffness. In addition, the strains measured by the strain gauges on the nail were recorded for the implantation procedure and during the static tests.

The effect of the fracture type on strains in the nail and stiffness of the construct was tested for significance by ANOVA and a Tukey HSD post hoc test. The correlation between the FE and the experimental results was tested

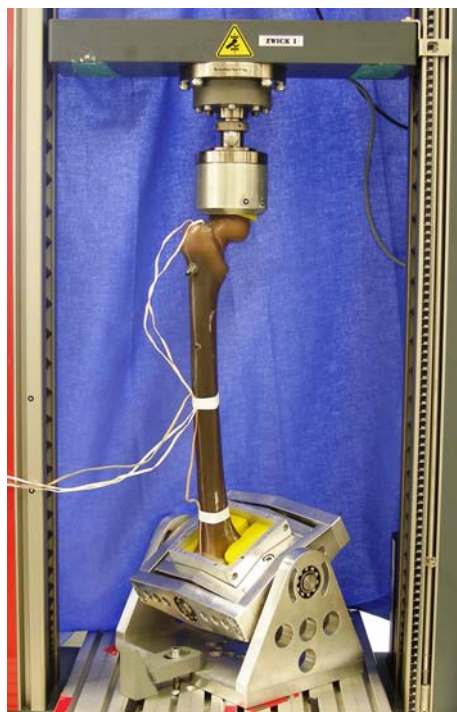


Fig. 4 The experimental setup with one specimen is shown.

Table 1. The testing sequence

Cycles	Type of Load	Start	Maximum	Holding Time	End
3	compression	0 N	300 N	0 min	0 N
3	compression	0 N	600 N	0 min	0 N
3	compression	0 N	900 N	0 min	0 N
3	compression	0 N	1200 N	0 min	0 N
3	compression	0 N	1500 N	0 min	0 N
2	compression	0 N	1866 N	0 min	0 N
1	compression	0 N	1866 N	4 min	0 N

with a Pearson test (SPSS for Windows, Rel. 14.0.1. 2005, SPSS Inc., Chicago, IL).

Results

The three different experimental groups produced different strains ($p < 0.001$) and stiffness values ($p = 0.043$) for each fracture type. The pertrochanteric fracture (Table 2) resulted in significantly ($p < 0.001$) higher strains than the lateral neck fracture in all three strain gauges. The subtrochanteric fracture (Table 2) displayed the highest ($p \leq 0.002$) strains in all three strain gauges at the maximum load. The lateral neck fracture (Table 2) exhibited a substantially higher stiffness than the pertrochanteric fracture ($p = 0.036$). Between the groups with the lateral neck and the subtrochanteric fracture ($p = 0.538$) and between the groups with the subtrochanteric and the pertrochanteric fracture ($p = 0.242$) no differences could be observed. However, the construct stiffness was quite similar (median 462–528 N/mm) for all three fracture types (Table 2).

The FE model displayed a considerable sensitivity to the implant position and the coefficient of friction in the fracture gap but a negligible sensitivity to the coefficient of friction between implant and bone. With an increasing coefficient of friction between the fracture fragments, the

Table 2. The strain and stiffness results for the experiments with the three fracture types

Fracture	Stiffness (N/mm)	Strain ($\mu\text{m/m}$)		
		SG 1	SG 2	SG 3
Petrochanteric A1.1				
Max	29	779	767	680
75th percentile	489	1715	1675	1638
Median	462	1413	1399	1227
25th percentile	430	1154	1274	1077
Min	102	633	261	204
Lateral Neck B2.1				
Max	37	925	638	164
75th percentile	552	-209	212	575
Median	528	-563	-61	473
25th percentile	511	-632	-196	387
Min	54	194	485	358
Subtrochanteric A3.2				
Max	126	282	455	142
75th percentile	519	2886	2536	2491
Median	469	2646	2358	2447
25th percentile	467	2459	2192	2371
Min	24	246	277	582

SG = Strain Gauge.

Table 3. The deviations and the correlation between the numerical and the experimental strain and stiffness data

Fracture	Stiffness (N/mm)	Strain ($\mu\text{m/m}$)		
		SG 1	SG 2	SG 3
Petrochanteric A1.1				
FEA	464	1774	1618	1008
Exp. (n = 6)	462	1413	1399	1227
Δ (%)	0	26	16	-18
Lateral Neck B2.1				
FEA	524	-144	-42	328
Exp. (n = 6)	528	-563	-61	473
Δ (%)	-1	-74	-31	-31
Subtrochanteric A3.2				
FEA	518	1807	2080	1999
Exp. (n = 6)	469	2646	2358	2447
Δ (%)	11	-32	-12	-18

SG = Strain Gauge; FEA = Finite Element Analysis; Exp. = Experiment; Δ (%) = $100 * (\text{FEA-Exp.})/\text{Exp}$; Mean of the amounts of deviations $\Delta \pm \text{SD} = 23 \pm 20\%$; Correlation $R^2 = 0.953$ ($p < 0.01$).

Table 4. The results by the numerical simulations

Fracture	Stiffness (N/mm)	von Mises Stress (MPa)	IFM (mm)	
			Axial	Shear
Petrochanteric A1.1	464	623	0,6	0,7
Lateral Neck B2.1	524	480	0,3	0,6
Subtrochanteric A3.2	518	665	0,4	0,1

IFM = interfracture movement. The stress values are the maximum von Mises stress values in regions of high tensile strain.

strains on the implants decreased (mean alteration -182%) and vice versa (mean alteration +76%). With the correct positioning of the implant, the correlation and the mean deviation for the strains and the construct stiffness between the FE models and the experimental results were rather good (Table 3).

In the simulations with the validated FE models, the fracture type affected the outcome of the strains but not of the construct stiffness. All three fractures resulted in similar values (464–524 N/mm) for the stiffness (Table 4). But the fracture type had an effect on the stress distribution within the implant. The petrochanteric fracture resulted in a lower stress (Fig. 5A) than the subtrochanteric fracture with even lower values for the lateral neck fracture. The lateral neck fracture displayed very low stresses at the lag screw hole (Fig. 5B) compared to the other two fractures and had its stress concentration spot at the middle of the lag screw (Fig. 5C). The subtrochanteric fracture resulted in the highest local stress observed at the lateral aspect near the lag screw hole (Fig. 5D).

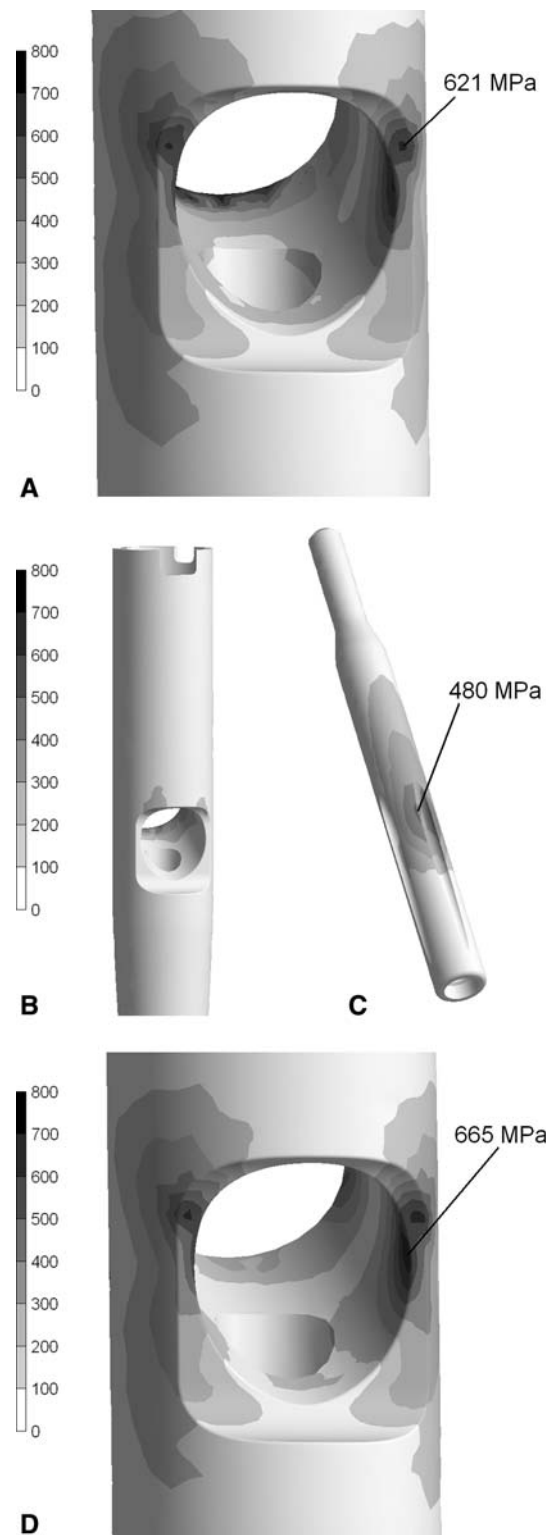


Fig. 5A–D The calculated von Mises stress distribution in MPa within the implant is shown. (A) The stress distribution within the proximal part of the nail for the petrochanteric fracture is illustrated. The stress distribution within the proximal part (B) and within the lag screw (C) for the lateral neck fracture is shown. (D) The stress distribution within the proximal part of the nail for the subtrochanteric fracture is shown. The values for the peak stress are given and marked by lines.

The interfragmentary movement (IFM) in the axial direction between the proximal and distal fragment was the highest in the model with a pertrochanteric fracture. Lower and almost equal IFM in the axial direction were attained by the two other fracture types. About the same overall picture emerged for the IFM in the transverse direction. The largest shear occurred in the pertrochanteric fracture followed by the lateral neck and the subtrochanteric fracture (Table 4).

During implantation of the nails into the Sawbones, an unanticipated result could be observed. The prestress of the nails measured by the strain gauges highly depended on the angle of insertion in the frontal plane. This finding was confirmed by the sensitivity study of the FE models.

Discussion

The choice of the appropriate implant continues to be critical for the fixation of unstable fractures of the hip. Therefore, a finite element model of the human femur was developed with three different fractures in the proximal region, stabilized by an intramedullary nail. The goal was to study the mechanical characteristics of hip fracture osteosynthesis with particular focus on the stiffness of the osteosynthesis, the stress distribution within the implant, and the interfragmentary movement in axial and transverse direction. Our hypothesis was that decreasing fracture stability results in increasing load share of the implant and therefore higher stress within the implant. We also asked how the IFM is related to the fracture stability.

Based on FE methodology, a numerical model was developed to study fractures of the proximal femur. The numerical model was validated with mechanical experiments and demonstrated reasonable accuracies for the calculation of local stress and overall constructs stiffness values. The three different fracture types examined demonstrated disparate load shares between the osteosynthesis implant and the fractured bone. While the overall construct stiffness was similar, the stress distributions and the fracture site motion heavily depended on the fracture type.

The pertrochanteric and the subtrochanteric fractures produced the largest stress concentration in the intramedullary implant at the lag screw hole, while the neck fracture produced lower stress values and a stress concentration at the lag screw. The stress was the highest in the subtrochanteric fracture due to the fact that the nail was pulled out of the distal fragment like a corkscrew pulls a cork out of a bottle. With the lever between the load and the contact area of the fracture fragments being several times larger than the lever between the contact area of the fracture fragments and the nail, this pulling force was several times higher than the load as well. This effect was less

pronounced for the pertrochanteric fracture and in the case of the lateral neck fracture the lag screw was sheared and the nail kept relatively unaffected. All calculated stresses were below the fatigue strength of the used alloy for 500,000 load cycles (Dindorf C. 'Ermüdung und Korrosion nach mechanischer Oberflächenbehandlung von Leichtmetallen' [Thesis] TU Darmstadt; 2006, unpublished data). Even in the absence of fracture healing the implants would not fail during the first 100 days after surgery, assuming 5000 cycles of walking per day [27].

The IFMs depended on the fracture type but to a greater extent on the fractures' orientation to the load vector. The pertrochanteric fracture resulted in the largest IFMs in the axial and transverse directions. This can be explained by the large fracture area, which had approximately a 45° angle to the load vector. That caused the proximal fragment to slide on the distal fragment and the fracture to open up. The lateral neck and the subtrochanteric fracture had similar amounts of stiffness and lower amounts of IFMs with the lowest values for the subtrochanteric fracture. The subtrochanteric fracture was nearly perpendicular to the load vector, which made it very insensitive to the load. With the fracture almost parallel to the load vector the lateral neck fracture resulted in a larger transversal than axial IFM.

Although the proximal strain gauges were placed symmetrically around the lag screw hole, they recorded different strain values. This can be explained by the angulation of the shaft axis in the sagittal plane and a small twist of the nail about its shaft-axis that occurred when the nail was inserted into the bone. The distal end of the nail slipped into the intramedullary canal and was forced into a position, which resulted in a twist of the nail. Generally the prestress of the nail depended highly on the angle of insertion achieved during the operative procedure.

The strains and the system stiffness for the FE models correlated well with the experimentally determined values, given that one model of each fracture type was compared to the median of the results of six experimental specimens. For the most strain or stiffness values the numerical results were in the range of the 25th to 75th percentile of the experimental results. Furthermore, the sensitivity study on the FE models demonstrated the same amount of variation (−182% to +76%) that could be observed in the experiments (−163% to +72%). So the models represented the results of the experimental groups rather good despite their variations. Important is the fact that the numerical models displayed the right tendency for each fracture and reflected the statistical differences between the fractures found in the experiments.

However, the FEA produced lower strain values in most cases. The deviations for the strains between FEA and measurements were −32% to +26%, except one value with a deviation of −74%. This sounds high, but the absolute deviation is about −420 µm/m. Generally and from a

technical point of view, the absolute deviations were small and can be compared to other studies in this field of research [11, 30, 31]. The deviations for stiffness were very small and the correlation was excellent. The mean deviation amounted to 28.5% for the strain values and 3.9% for the stiffness values respectively.

The strength of this study is the model's potential to study the mechanical performance of hip fractures. The model is easily adjustable for various fracture types, osteosynthesis devices, and loading scenarios and it is well-validated for a range of fracture types. So far there are very few studies that investigated the mechanical performance with a numerical model that has been validated by strain measurements on an implanted intramedullary nail [6].

However, this study has some limitations. The lateral neck and the subtrochanteric fracture have to be considered as borderline cases or even contraindications for the short Gamma3 nail used in this study. Choosing these two fractures had the purpose of generating dissimilar stress and strain distributions in the implant and study the model for a large range of fracture types. Furthermore, artificial bones were used instead of cadaver bones. It is known that the fourth-generation Sawbones are very close to human bones regarding their mechanical properties [7, 8]. However, they present a young and healthy population and not a very broad cross-section of the population in terms of mechanical properties. Nevertheless, the goal of this study was to build a model of a standardized femur that was able to be validated. A standardized model has the advantage of making implants and fractures comparable while the bone parameters stay constant and the results are highly reproducible. The validated model can easily be adapted to different material properties of the cortical and cancellous bone to simulate osteoporotic bones. However, it currently cannot simulate the wall thinning of cortical bone, which could be a future task.

The load scenario used focused solely on the hip force. Muscle forces were not considered. This was due to the process of validation. It is very complex to accomplish experiments on a regular testing machine with more than one force acting on the bone. In addition, the loading with a single hip force can be considered a worst case scenario. It is known that the resulting force of the muscle forces acting on the lateral side of the major trochanter reduces the bending of the femur in the frontal plane [22]. Simoes et al. confirmed this behavior by measuring lower strains on the femur, when adding muscle forces to the loading scenario [28]. It can be concluded that a single hip force results in the largest bending of the femur and therefore the whole osteosynthesis compared to a loading scenario with added muscle forces. Another limitation is the use of only one implant. Nevertheless the Gamma3 nail is very representative of cephalocondylic intramedullary nails.

The results of this study are consistent with the current literature. Although the three fractures tested exhibited different initial stabilities, the stiffness of the whole osteosynthesis construct was typically very similar [3, 15, 23]. Although the subtrochanteric fracture is considered highly unstable, it did not result in a substantially lower stiffness than the other two fractures. However, the load on the implant increased with decreasing fracture stability and resulted in higher strains and higher stresses on the implant [3, 5, 16, 17, 26]. Thus, intramedullary implants can stabilize unstable hip fractures with almost the same amount of stiffness as seen in stable fractures, but they have to bear a higher load share, which results in higher stresses in the implant. These higher stresses could cause fatigue failure, particularly in the case of delayed or absent fracture healing.

The FE model is capable of comparing various fractures and implants regarding the osteosynthesis stiffness, the stress distribution in the implant and the IFM. Thus the choice of an implant for specific fractures, especially unstable fractures, can be based on quantifiable mechanical markers. Future implants could be optimized towards meeting the mechanical demands of hip fractures. Furthermore, the model is able to clarify which fractures are stable or unstable.

Acknowledgments We thank Roman Brunner for his support during the experimental stage of the study and Florian Högel, MD, for his support during the surgical procedures.

References

1. Audige L, Hanson B, Swiontkowski MF. Implant-related complications in the treatment of unstable intertrochanteric fractures: meta-analysis of dynamic screw-plate versus dynamic screw-intramedullary nail devices. *Int Orthop*. 2003;27:197–203.
2. Bergmann G, Deuretzbacher G, Heller M, Graichen F, Rohlmann A, Strauss J, Duda GN. Hip contact forces and gait patterns from routine activities. *J Biomech*. 2001;34:859–871.
3. Bostrom MP, Lyden JP, Ernberg JJ, Missri AA, Berberian WS. A biomechanical evaluation of the long stem intramedullary hip screw. *J Orthop Trauma*. 1995;9:45–52.
4. Breuil V, Roux CH, Testa J, Albert C, Chassang M, Brocq O, Euller-Ziegler L. Outcome of osteoporotic pelvic fractures: An underestimated severity. Survey of 60 cases. *Joint Bone Spine*. 2008;75:585–588.
5. Chang WS, Zuckerman JD, Kummer FJ, Frankel VH. Biomechanical evaluation of anatomic reduction versus medial displacement osteotomy in unstable intertrochanteric fractures. *Clin Orthop Relat Res*. 1987;141–146.
6. Cheung G, Zalzal P, Bhandari M, Spelt JK, Papini M. Finite element analysis of a femoral retrograde intramedullary nail subject to gait loading. *Med Eng Phys*. 2004;26:93–108.
7. Chong AC, Friis EA, Ballard GP, Czuwala PJ, Cooke FW. Fatigue performance of composite analogue femur constructs under high activity loading. *Ann Biomed Eng*. 2007;35:1196–1205.

8. Chong AC, Miller F, Buxton M, Friis EA. Fracture toughness and fatigue crack propagation rate of short fiber reinforced epoxy composites for analogue cortical bone. *J Biomech Eng.* 2007;129:487–493.
9. Cooper C, Campion G, Melton LJ, III. Hip fractures in the elderly: a world-wide projection. *Osteoporos Int.* 1992;2:285–289.
10. Cornwall R, Gilbert MS, Koval KJ, Strauss E, Siu AL. Functional outcomes and mortality vary among different types of hip fractures: a function of patient characteristics. *Clin Orthop Relat Res.* 2004;425:64–71.
11. Cristofolini L, Viceconti M, Cappello A, Toni A. Mechanical validation of whole bone composite femur models. *J Biomech.* 1996;29:525–535.
12. Eveleigh RJ. A review of biomechanical studies of intramedullary nails. *Med Eng Phys.* 1995;17:323–331.
13. Gourlay M, Richey F, Reginster JY. Strategies for the prevention of hip fracture. *Am J Med.* 2003;115:309–317.
14. Gullberg B, Johnell O, Kanis JA. World-wide projections for hip fracture. *Osteoporos Int.* 1997;7:407–413.
15. Kummer FJ, Olsson O, Pearlman CA, Ceder L, Larsson S, Koval KJ. Intramedullary versus extramedullary fixation of subtrochanteric fractures. A biomechanical study. *Acta Orthop Scand.* 1998;69:580–584.
16. Mahomed MN, Harrington IJ, Hearn TC. Biomechanical analysis of the Medoff sliding plate. *J Trauma.* 2000;48:93–100.
17. Meislin RJ, Zuckerman JD, Kummer FJ, Frankel VH. A biomechanical analysis of the sliding hip screw: the question of plate angle. *J Orthop Trauma.* 1990;4:130–136.
18. Morlock M, Schneider E, Bluhm A, Vollmer M, Bergmann G, Muller V, Honl M. Duration and frequency of every day activities in total hip patients. *J Biomech.* 2001;34:873–881.
19. Morrison JB. The mechanics of the knee joint in relation to normal walking. *J Biomech.* 1970;3:51–61.
20. Nuno N, Amabili M, Groppetti R, Rossi A. Static coefficient of friction between Ti-6Al-4V and PMMA for cemented hip and knee implants. *J Biomed Mater Res.* 2002;59:191–200.
21. Pajarinen J, Lindahl J, Savolainen V, Michelsson O, Hirvensalo E. Femoral shaft medialisation and neck-shaft angle in unstable pertrochanteric femoral fractures. *Int Orthop.* 2004;28:347–353.
22. Pauwels F, Furlong RJ, Maquet P. *Biomechanics of the Normal and Diseased Hip.* Berlin, Germany: Springer; 1976.
23. Ramer M, Viceconti M, Toni A, Pipino F, Giunti A. Biomechanical validation of a new nail-plate for the repair of stable proximal femoral fractures. *Arch Orthop Trauma Surg.* 1997;116:137–142.
24. Raunest J, Engelmann R, Jonas M, Derra E. Morbidity and mortality in para-articular femoral fractures in advanced age. Results of a prospective study. *Unfallchirurg.* 2001;104:325–332.
25. Roberts CS, Nawab A, Wang M, Voor MJ, Seligson D. Second generation intramedullary nailing of subtrochanteric femur fractures: a biomechanical study of fracture site motion. *J Orthop Trauma.* 2002;16:231–238.
26. Rosenblum SF, Zuckerman JD, Kummer FJ, Tam BS. A biomechanical evaluation of the Gamma nail. *J Bone Joint Surg Br.* 1992;74:352–357.
27. Schmalzried TP, Szuszczewicz ES, Northfield MR, Akizuki KH, Frankel RE, Belcher G, Amstutz HC. Quantitative assessment of walking activity after total hip or knee replacement. *J Bone Joint Surg Am.* 1998;80:54–59.
28. Simoes JA, Vaz MA, Blatcher S, Taylor M. Influence of head constraint and muscle forces on the strain distribution within the intact femur. *Med Eng Phys.* 2000;22:453–459.
29. Verhofstad MH, van der Werken C. DHS osteosynthesis for stable pertrochanteric femur fractures with a two-hole side plate. *Injury.* 2004;35:999–1002.
30. Yosibash Z, Padan R, Joskowicz L, Milgrom C. A CT-based high-order finite element analysis of the human proximal femur compared to in-vitro experiments. *J Biomech Eng.* 2007;129:297–309.
31. Yosibash Z, Trabelsi N, Milgrom C. Reliable simulations of the human proximal femur by high-order finite element analysis validated by experimental observations. *J Biomech.* 2007;40:3688–3699.